Magnetic Characteristic Analysis of Permanent Magnet Motor with Complex E&S Modeling

Shingo Zeze *, Takashi Todaka * and Masato Enokizono *

Abstract – This paper presents analyzed results of a permanent magnet motor by using complex E&S modeling. The calculated results are compared with ones from the conventional E&S modeling for verification. Combinations of the numbers of slots and poles are investigated to reduce total iron loss. The results demonstrate that the complex E&S modeling is very useful in design under consideration of rotational magnetic field and magnetic anisotropy.

Keywords: Complex E&S Modeling, Vector Magnetic Properties, jω Method, PM Motor, Finite Element Method

1. Introduction

In order to develop high-efficiency electrical machines, it is necessary to consider accurate magnetic properties in the structural design. Recently, techniques for measuring vector magnetic properties have been developed and their achievements have drawn much attention. Fig. 1 shows the relationship between the flux density vector ***B*** and the field strength vector ***H***. The vector magnetic properties enable us to know the rotational iron loss distributions and magnetic anisotropic properties from the relationship between ***B*** and ***H*** [1]-[4].

The vector magnetic properties accurately represent the magnetic properties of various kinds of electrical steel sheets. We proposed the E&S modeling to consider the vector magnetic properties in magnetic field analyses. However, the E&S modeling is very time-consuming. To solve this problem, we proposed a complex E&S modeling with assumption that both flux density and field strength waveforms are sinusoidal. The computation time of the complex E&S modeling is 1/10 in comparison with one of the conventional types of E&S modeling [1].

We have carried out a magnetic characteristic analysis of a surface permanent magnet motor, by combining the finite element method and the complex E&S modeling, to develop high-efficiency machines. The combinations of the numbers of slots and poles are investigated with three models and the iron loss distributions are compared. In this paper, knowledge obtained in the numerical simulations is reported.

* Dept. of Electrical and Electronic Engineering, Oita University, Japan. (v10f1002@oita-u.ac.jp)

Received 17 June 2011 ; Accepted 12 October 2011

2. Two-Dimensional Magnetic Property

It is well known that ***B*** and ***H*** are usually not parallel in magnetic materials. However, this property has been neglected in technical designing so far because of the difficulty in obtaining magnetic measurements. The Epstein method and the SST testing method are well known standard measurement methods of the one-dimensional magnetic properties. In obtaining these measurements, it is required that ***B*** and ***H*** be parallel to each other. These measurement methods are the IEC international standard for commercial use. Thus, the measurement accuracy is not so important. Practically, phase difference between ***B*** and ***H*** exists and it varies depending on the direction of ***B***. In other words, nonlinearities exist not only in magnitude of ***B***, but also in direction of ***B***. The property that considers the magnitude and direction of ***B*** and ***H*** is called the two-dimensional vector magnetic property and it expresses the vector relationship between ***B*** and ***H*** accurately [2], [3].

Fig. 2 shows the alternating magnetic flux condition and the rotating magnetic flux condition, respectively. The vector magnetic properties are defined by the maximum magnetic flux density B_{max}, the inclination angle θ_B, and the axis ratio α. For the case of the precise circular rotating flux, α equals one, and for the case of the alternating flux, α equals zero.

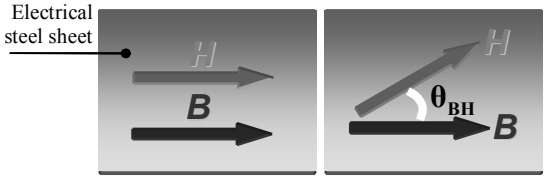

Fig. 1. Relationship between ***B*** and ***H***

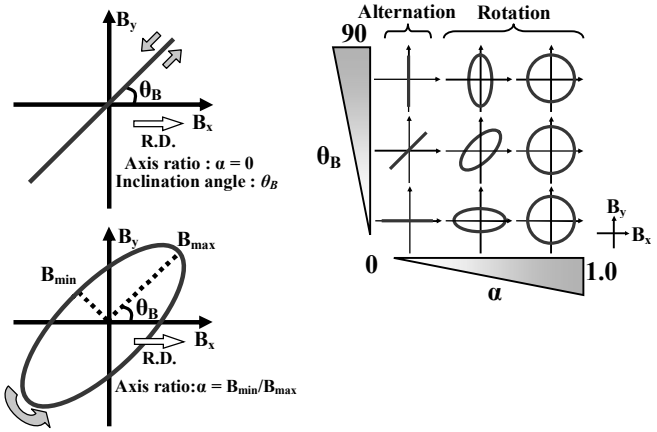

Fig. 2. Alternating and rotating flux conditions

3. Complex Type E&S Modeling

2.1 Conventional E&S modeling

The conventional E&S modeling is expressed as follows:

$$\begin{cases} H_x = \nu_{xr} B_x + \nu_{xi} \dfrac{\partial B_x}{\partial t} \\ H_y = \nu_{yr} B_y + \nu_{yi} \dfrac{\partial B_y}{\partial t} \end{cases} \tag{1}$$

where ν_{xr}, ν_{yr} are the magnetic reluctivity coefficients, and ν_{xi}, ν_{yi} are the magnetic hysteresis coefficients.

2.2 Complex E&S Modeling

If the magnetic flux density and field strength waveforms are both sinusoidal, the time derivative can be replaced by the complex number, jω. As a result, the complex E&S modeling can be expressed as follows:

$$\begin{cases} \dot{H}_x = \left(\bar{\nu}_{xr} + j\omega \bar{\nu}_{xi}\right) \dot{B}_x \\ \dot{H}_y = \left(\bar{\nu}_{yr} + j\omega \bar{\nu}_{yi}\right) \dot{B}_y \end{cases} \tag{2}$$

where $\bar{\nu}_{xr}, \bar{\nu}_{yr}$ are the effective magnetic reluctivity coefficients, and $\bar{\nu}_{xi}, \bar{\nu}_{yi}$ are the effective magnetic hysteresis coefficients. The variables denoted with a dot are complex variables. The magnetic flux densities and the magnetic field strengths are expressed by the following equations, where the given phase relationships are as shown in Fig. 3:

$$\begin{cases} \dot{B}_x = \left|\dot{B}_x\right| e^{j\theta_{B_x}} = \left|\dot{B}_x\right| (\cos\theta_{B_x} + j\sin\theta_{B_x}) \\ \dot{B}_y = \left|\dot{B}_y\right| e^{j\theta_{B_y}} = \left|\dot{B}_y\right| (\cos\theta_{B_y} + j\sin\theta_{B_y}) \\ \dot{H}_x = \left|\dot{H}_x\right| e^{j\theta_{H_x}} = \left|\dot{H}_x\right| (\cos\theta_{H_x} + j\sin\theta_{H_x}) \\ \dot{H}_y = \left|\dot{H}_y\right| e^{j\theta_{H_y}} = \left|\dot{H}_y\right| (\cos\theta_{H_y} + j\sin\theta_{H_y}) \end{cases} \tag{3}$$

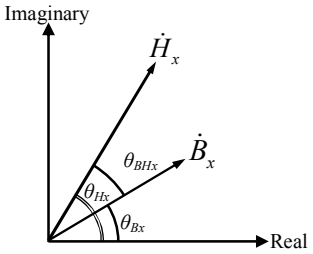

Fig. 3. Definition of phase relationship

Substituting equation (3) into equation (2), the effective magnetic reluctivity and magnetic hysteresis coefficients are given by:

$$\begin{cases} \bar{\nu}_{xr} = \dfrac{\left|\dot{H}_x\right|}{\left|\dot{B}_x\right|} \cos(\theta_{BH_x}), \bar{\nu}_{xi} = \dfrac{\left|\dot{H}_x\right|}{\omega\left|\dot{B}_x\right|} \sin(\theta_{BH_x}) \\ \bar{\nu}_{yr} = \dfrac{\left|\dot{H}_y\right|}{\left|\dot{B}_y\right|} \cos(\theta_{BH_y}), \bar{\nu}_{yi} = \dfrac{\left|\dot{H}_y\right|}{\omega\left|\dot{B}_y\right|} \sin(\theta_{BH_y}) \end{cases} \tag{4}$$

2.3 Governing and Finite Element Equations

The governing equation under consideration of the complex E&S modeling can be expressed by:

$$\begin{aligned} &\frac{\partial}{\partial x}\left(\bar{\nu}_{yr} \frac{\partial \dot{A}_z}{\partial x} + j\omega \bar{\nu}_{yi} \frac{\partial \dot{A}_z}{\partial x}\right) \\ &+ \frac{\partial}{\partial y}\left(\bar{\nu}_{xr} \frac{\partial \dot{A}_z}{\partial y} + j\omega \bar{\nu}_{xi} \frac{\partial \dot{A}_z}{\partial y}\right) = -\dot{J}_{0z} \end{aligned} \tag{5}$$

The finite element equation for equation (5) can be given by:

$$\begin{aligned} &\iint_s \left[\sum_{j=1}^{3} \left[\begin{aligned} &\left\{ \frac{C_{ie}}{2\Delta}\left(\bar{\nu}_{yr} \frac{C_{ie}}{2\Delta}\right) \frac{D_{ie}}{2\Delta}\left(\bar{\nu}_{xr} \frac{D_{ie}}{2\Delta}\right) \right\} \\ &+ j\omega \left\{ \frac{C_{ie}}{2\Delta}\left(\bar{\nu}_{yi} \frac{C_{ie}}{2\Delta}\right) \frac{D_{ie}}{2\Delta}\left(\bar{\nu}_{xi} \frac{D_{ie}}{2\Delta}\right) \right\} \end{aligned} \right] \dot{A}_{je} \right] dxdy \\ &- \dot{J}_0 = 0 \end{aligned} \tag{6}$$

where x and y are coordinates, and Δ is the area of the linear triangular elements. The subscripts, ie, je, ke, are the node numbers at corner points of a triangular element.

2.4 Iron Loss Calculation

The iron loss P_{ti} [W/kg] of each finite element i can be calculated directly with the following equation, without using an approximated function, based on measured data:

$$P_{ti} = \left| \frac{1}{\rho T} \int_C \vec{H} \cdot d\vec{B} \right| \tag{7}$$

where ρ is the core material density, and T is the period of the exciting waveform.

The iron loss P_{ti} corresponds to the total area of the hysteresis loop over the x- and y-directions. Therefore, the total iron loss P_{total} [W] is given by

$$P_{total} = \rho \cdot D_P \cdot N_{os} \cdot \sum_{i=1}^{Nes} P_{ti} \cdot S_i \tag{8}$$

(Note to authors: What is S_i?)

where D_P is the thickness of the electrical steel sheet, N_{os} is the number of laminations of the sheet, and N_{es} is the number of finite elements. The specimen used in the analysis was assumed to be silicon steel sheet (50A470, D_P = 0.5 mm, ρ = 7700 kg/m^3).

2.5 Applicable Range

The magnetic flux density and the magnetic field strength waveforms are both sinusoidal in the complex E&S modeling. Therefore, it is necessary to make clear the range over which complex E&S modeling is applicable. Fig. 4 shows the original and approximated hysteresis loops under alternating flux conditions (θ_B = 0, 90 deg) and Fig. 5 shows the areas of the hysteresis loops (iron loss). In the case of low magnetic flux conditions, the iron losses of the original and approximated loops were in agreement. However, the iron loss difference became larger when the waveforms were distorted under high flux density conditions. Fig. 6 shows the initial magnetization curves of R.D. (rolling direction) and T.D. (transverse direction). The applicable range of the complex E&S modeling can be considered to be the area of low magnetic flux density conditions, below 1.1 T.

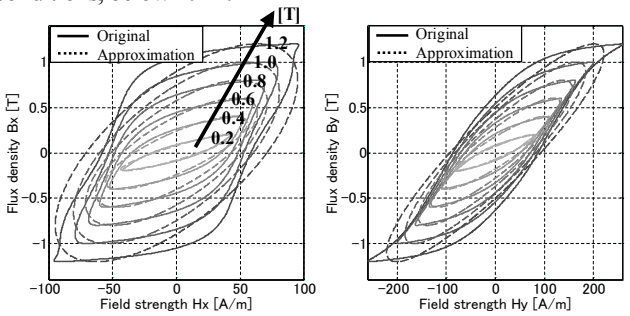

(a) θ_B = 0 deg (b) θ_B = 90 deg

Fig. 4. Hysteresis loops for B_{max} = 0.2 T to 1.2 T, α = 0

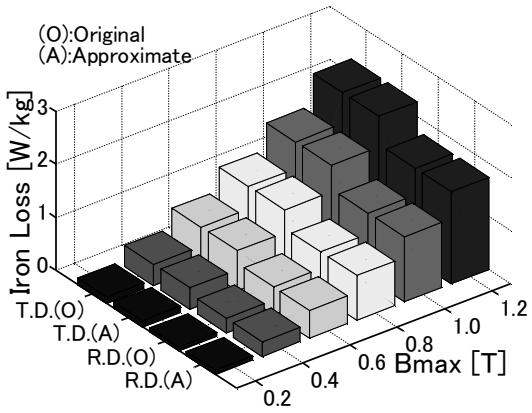

Fig. 5. Comparison of the original hysteresis loops with the approximated ones

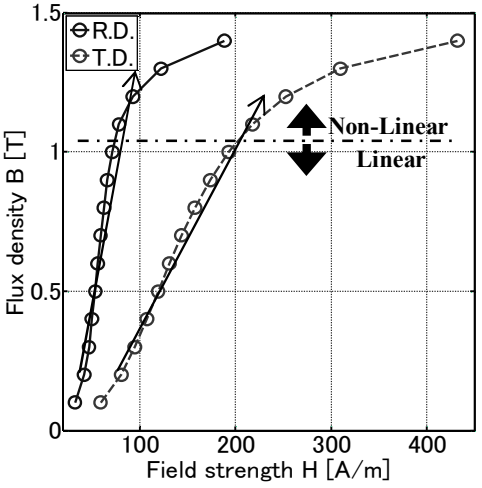

Fig. 6. Initial magnetization curves of R.D. and T.D.

2.6 Flow Chart

Fig. 7 shows the flow chart of this analysis. Fig. 8 shows the motor model core and the method to set boundary conditions on the center line of the air gap. The region analyzed with the complex E&S modeling included only the stator, including the outer air region. As the rotating direction is CCW, the boundary conditions are given by (9), where $\dot{A}$ is the complex vector potential, which can be generated by the permanent magnets on the rotor surface.

Because the components of the reluctivity coefficients are nonlinear, iterative calculation is necessary. We can carry out the non-linear magnetic field analysis considering both alternating and rotating hysteresis with this modeling. From the results of simulations, we can obtain directly the iron loss distributions in the stator core.

$$\dot{A} = A_{\max} \left(\cos\theta_P + i \cdot \sin\theta_P \right) \tag{9}$$

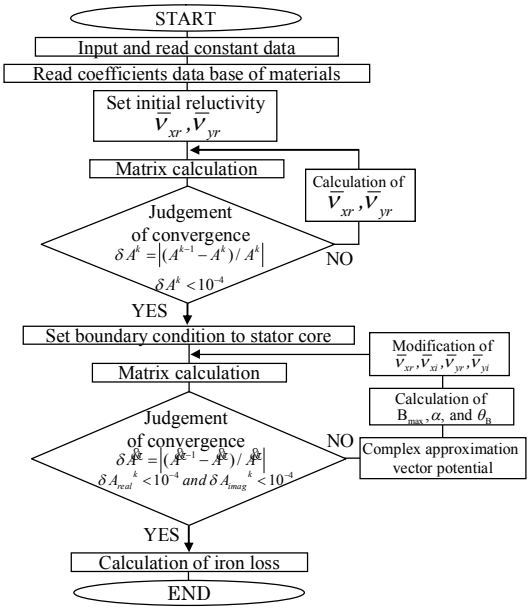

Fig. 7. Flow chart

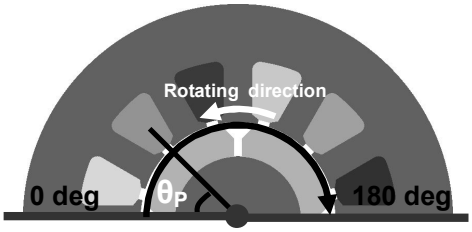

Fig. 8. Method of setting boundary conditions on the center line in the air gap

3. Permanent Magnet Motor Model

Fig. 9 shows the permanent magnet motor models used in the analysis. As shown in Fig. 9, three-phase stator windings were distributed. Table 1 shows the conditions used in the analysis. The numbers of slots in the stator cores were 6, 12, and 18; and the number of poles in the rotors was 4. The exciting current and frequency were 0 A (No-load) and 50 Hz, respectively. The magnetization of the magnet was 0.2 T.

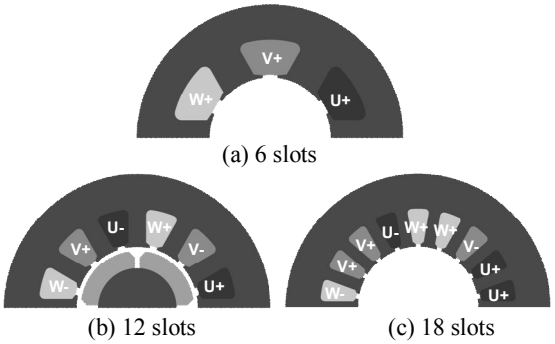

(a) 6 slots

(b) 12 slots (c) 18 slots

Fig. 9. Analyzed models

Table 1. Conditions used in the analysis

Outer diameter of the stator core	53.4 mm
Outer diameter of the rotor core	22.6 mm
Gap length	0.5 mm
Number of turns in the exciting coils	200, 100, 66 turns/slot
Electrical steel sheet	50A470
Exciting current	0 A
Residual magnetization	0.2 T
Revolution speed	1500 min^{-1}
Rolling direction	0 deg

4 Results and Discussions

Figs. 10, 11, and 12 show the distributions of the maximum magnetic flux density and magnetic flux, the maximum magnetic field strength, and the iron loss, respectively. Although some differences are seen, the distributions of the complex E&S modeling are in close agreement with those of the conventional E&S modeling. Fig. 13 shows the relative errors of the iron loss distributions. A large difference can be observed in the back yoke region and at the roots of the teeth. Fig. 14 shows the maximum magnetic flux density distribution and its variations are indicated in color. Fig. 15 shows the region where the relative error of the iron loss is less than 10%. It can be seen that the relative error of the iron loss becomes larger in the low magnetic flux density regions. This is due to the relative difference of the converged magnetic flux densities in each model. However, the absolute error is small. From this analysis, it can be said that the complex E&S modeling and the conventional E&S modeling correspond well overall. Fig. 16 shows the comparison of the total iron loss for each model. The increasing tendencies of the iron loss in each modeling are in good agreement.

5. Conclusion

This paper presented analyzed magnetic characteristics of the surface permanent magnet motor that were obtained by using the complex E&S modeling. The analysis of the permanent motor was enabled by using the proposed analysis technique, which used jω method. The results were compared with ones of the conventional E&S modeling and a good agreement between the two was demonstrated. In this analysis, the computation time was reduced to 1/20 of that required by the conventional modeling.

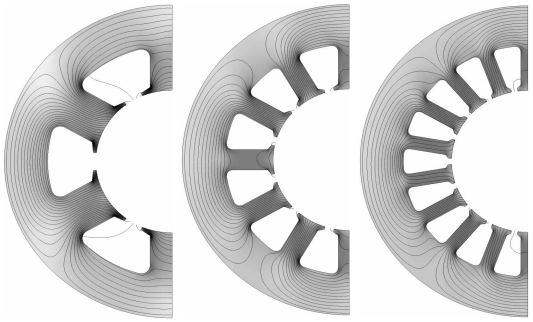

(a) Complex E&S modeling

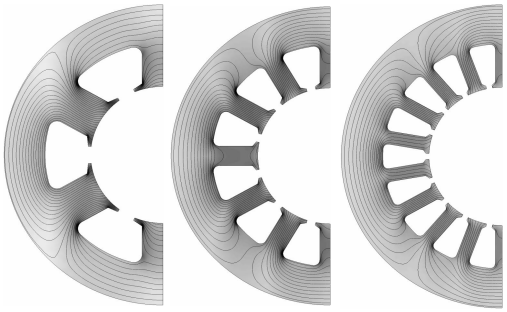

(b) Conventional E&S modeling

Fig. 10. Distributions of the magnetic flux and the maximum magnetic flux density

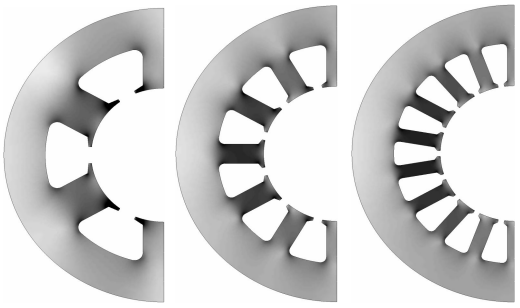

(a) Complex E&S modeling

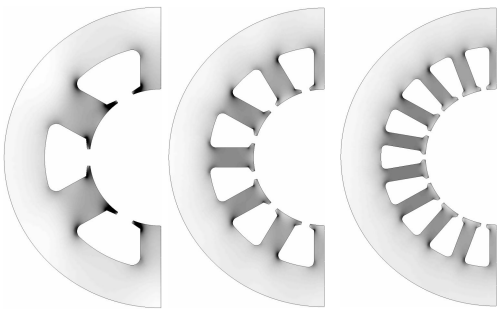

(b) Conventional E&S modeling

Fig. 11. Distributions of the maximum field strength

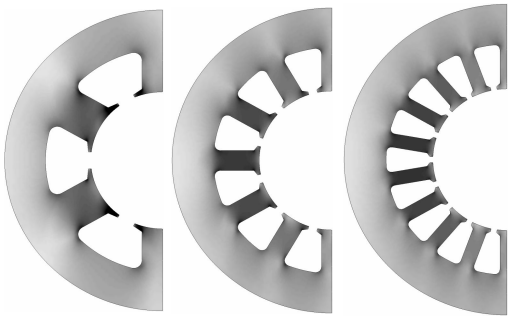

(a) Complex E&S modeling

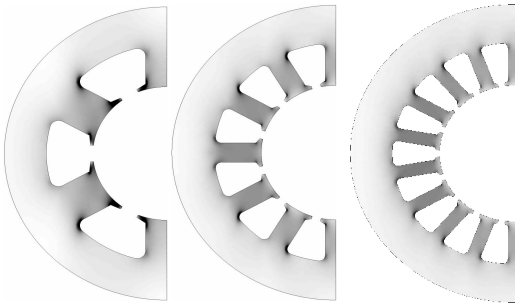

(b) Conventional E&S modeling

Fig. 12. Iron loss distributions

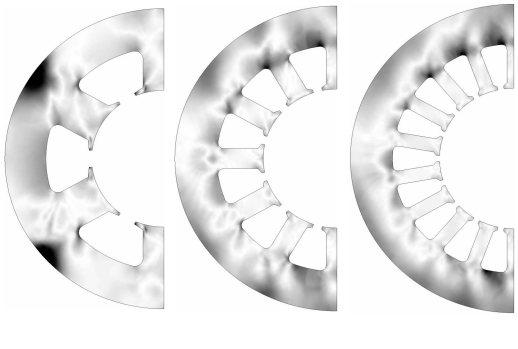

Fig. 13. Relative error of the iron loss distributions

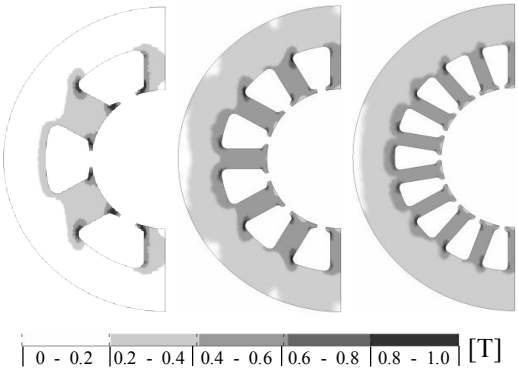

Fig. 14. Distributions of the maximum magnetic flux density that make the colors in each section the same

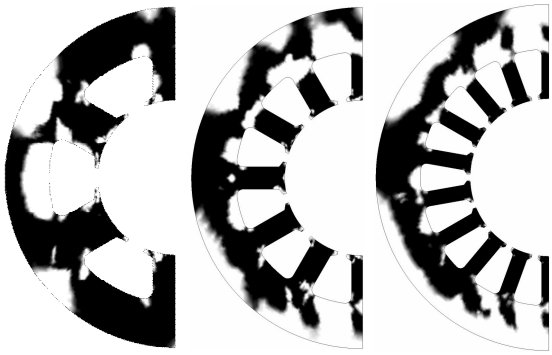

Fig. 15. Regions where the relative error of iron loss is less than 10 %

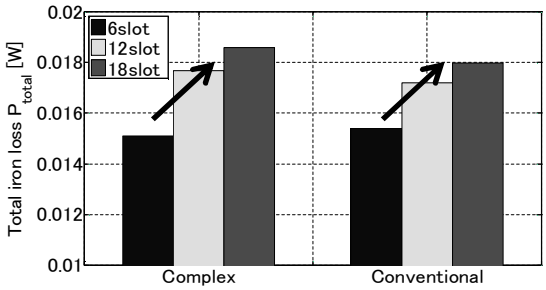

Fig. 16. Comparison of the iron loss, between of the Complex modeling case and the conventionl Modeling case, for each number of solts

References

[1] T. Todaka, K.Nakanoue and M.Enokizono, "Magnetic field analysis under complex approximation taking account of two-dimensional magnetic properties", *The International Journal for Computation and Mathematics in Electrical and Electronic Engineering*, Vol. 28, No. 1, pp. 98-108, 2009.

[2] N. Soda and M. Enokizono, "Improvement of T-joint part constructions in three-phase transformer cores by using direct loss analysis with E&S model," *IEEE Trans. Magn.*, vol.MAG-36, pp. 1724-1727, July 2000.

[3] M. Enokizono and N. Soda, "Direct magnetic loss analysis by FEM considering vector magnetic properties," *IEEE Trans. Magn.*, vol.34, pp. 188-195, Sept. 1998.

[4] Y. Maeda, T. Todaka, H. Simoji, M. Enokizono and J. Sievert, "An evaluation method of cross-type H-coil angle for accurate two-dimensional vector magnetic measurement", *Journal of Magnetism and Magnetic Materials*, Vol. 304, Issue 2, pp.564-567, September 2006.

[5] Kohsaka.T, Takahashi.N, Nogawa.S, Kuwata.M : "Analysis of magnetic characteristics of three-phase reactor made of grain-oriented silicon steel", *IEEE Trans. Magn.*, Vol.36, No.4, p.1894-1897 (2000)

[6] Nakano.M, Nishimoto.H, Fujiwara.K, Takahashi.N : "Improvements of single sheet testers for measurement of 2-D magnetic properties up to high flux density", *IEEE Trans. Magn.*, Vol.35, No.5, p.3965-3967 (1999)

[7] Mori.K, Yanase.S, Okazaki.Y, Hashi.S. : "2-D magnetic rotational loss of electrical steel at high magnetic flux density", *IEEE Trans. Magn.*, Vol.41, No.10, p.3310-3312 (2005)

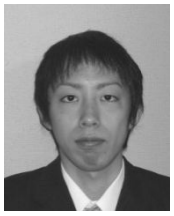

Shingo Zeze was born in 1985. He received the M.Eng. degree in electrical engineering from Oita University, Japan in 2010. He is currently a doctor's course student at Oita University, Japan.

Takashi Todaka was born in 1960. He is currently an Associate Professor at Department of Electrical and Electronic Engineering, Faculty of Engineering at Oita University, Japan. His main research area is in magnetic engineering. His recent research includes the development of a ferro-magnetic shape memory alloy and the study of its applications.

Masato Enokizono was born in 1949. He is currently a Professor at Department of Electrical and Electronic Engineering, Faculty of Engineering at Oita University, Japan. He received the research scholarship of Alexander von Humboldt-Stifung in the Phusikalisch-Technischen Bundesanstalt (PTB) Braunschweig Lab.